Investigating the reactivity of neutral water-soluble Ru(II)-PTA carbonyls towards the model imine ligands pyridine and 2,2′-bipyridine.

Federica Battistin,[a*†] Alessio Vidal,[a] Gabriele Balducci,[a] Enzo Alessio[a*]

[a] Department of Chemical and Pharmaceutical Sciences, University of Trieste, Via L. Giorgieri 1, 34127 Trieste, Italy.

[†] now at IMDEA Nanociencia, Faraday 9, Ciudad Universitaria de Cantoblanco, 28049 Madrid, Spain.

Supporting Information

Characterization of *trans*-[RuCl$_2$(bpy)(CO)(PTA)] (**11**).

Figure S1. X-ray molecular structure (50% probability ellipsoids) of *trans*-[RuCl$_2$(bpy)(CO)(PTA)]·H$_2$O (**11**·H$_2$O).

Figures S2-S4. NMR characterization in D$_2$O of *trans,trans,trans*-[RuCl$_2$(CO)(py)(PTA)$_2$] (**7**).

Figure S5. ^{1}H and ^{31}P{^{1}H} NMR spectra in D$_2$O of the mixture of *trans,trans,trans*-[RuCl$_2$(CO)(py)(PTA)$_2$] (**7**) and *cis,cis,trans*-[RuCl$_2$(CO)(py)(PTA)$_2$] (**8**) obtained by treatment of **2** with a slight excess of pyridine in chloroform.

Figures S6-S7. NMR characterization in CDCl$_3$ of *cis,cis,trans*-[RuCl$_2$(CO)$_2$(py)(PTA)] (**9**).

Figures S8-S12. NMR characterization in D$_2$O of *cis,trans*-[Ru(bpy)Cl(CO)(PTA)$_2$]Cl (**10**).

Figures S13-S15. NMR characterization in DMSO-*d$_6$* of *trans,cis*-[Ru(bpy)Cl$_2$(CO)PTA] (**11**).

Figures S16-S23. NMR characterization in D$_2$O of *mer*-[Ru(bpy)(CO)(PTA)$_3$]Cl$_2$ (**12**).

Figures S24-S26. NMR characterization in D$_2$O of *cis,trans*-[Ru(bpy)(CO)$_2$Cl(PTA)]Cl (**13**).

Figures S27-S29. NMR characterization in D$_2$O of *cis,trans*-[Ru(bpy)(CO)$_2$(PTA)$_2$](NO$_3$)$_2$ (**14NO$_3$**).

Figures S30-S34. NMR characterization in D$_2$O of *cis,cis*-[Ru(bpy)Cl(CO)(PTA)$_2$]Cl (**15**).

Figure S35. ^{31}P{^{1}H} NMR spectrum in D$_2$O of *cis,cis*-[Ru(bpy)(CO)$_2$Cl(PTA)]Cl (**15**) in 6/1 mixture with *cis,cis*-[Ru(bpy)Cl(CO)(PTA)$_2$]Cl (**16**) and some minor impurities.

Figure S36. Low-quality X-ray molecular structure (50% probability ellipsoids) of *cis,cis,trans*-[RuCl$_2$(CO)$_2$(py)(PTA)] (**9**).

Table S1. Selected CO stretching bands for compounds **7**, **9**, **10**, **12 - 16**. (cm^{-1}).

Table S2. Crystallographic data and refinement details for compounds *trans,trans,trans*-[RuCl$_2$(CO)(py)(PTA)$_2$] (**7**), *trans,cis*-[Ru(bpy)Cl$_2$(CO)PTA] (**11**), and *mer*-[Ru(bpy)(CO)(PTA)$_3$]Cl$_2$ (**12**)

Table S3. Selected coordination distances (Å) and angles (°) for *trans,trans,trans*-[RuCl$_2$(CO)(py)(PTA)$_2$] (**7**).

Table S4. Selected coordination distances (Å) and angles (°) for *trans*-[Ru(bpy)Cl$_2$(CO)PTA]·H$_2$O (**11**).

Table S5. Selected coordination distances (Å) and angles (°) for *mer*-[Ru(bpy)(CO)(PTA)$_3$]Cl$_2$·7H$_2$O (**12**).

Characterization of *trans*-[RuCl$_2$(bpy)(CO)(PTA)] (11)

A few crystals of *trans*-[RuCl$_2$(bpy)(CO)(PTA)] (**11**) spontaneously and slowly grew from the D$_2$O NMR solution of the raw product *cis,trans*-[Ru(bpy)Cl(CO)(PTA)$_2$]Cl (**10**), obtained from the reaction between *trans,trans,trans*-[RuCl$_2$(CO)(OH$_2$)(PTA)$_2$] (**1**) and bpy in refluxing water (Figure S1).
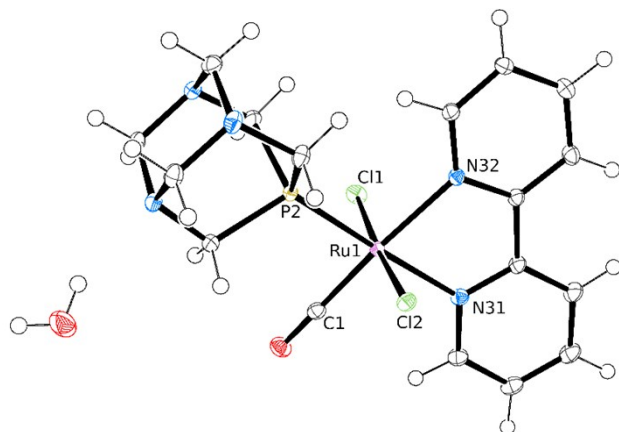

Figure S1. X-ray molecular structure (50% probability ellipsoids) of *trans*-[RuCl$_2$(bpy)(CO)(PTA)]·H$_2$O (**11**·H$_2$O). Coordination distances (Å): Ru1–C1 = 1.842(2), Ru1–Cl11 = 2.417(2), Ru1–Cl12 = 2.402(1), Ru1–N31 = 2.134(2), Ru1–N32 = 2.154(1), Ru1–P2 = 2.305(1).

This compound is most likely a side product of the reaction, that is formed when bpy replaces the water molecule and an adjacent PTA of **1** (rather than a Cl). The relatively low solubility of **11** in water is consistent with what observed with *cis,cis,trans*-[RuCl$_2$(CO)$_2$(py)(PTA)] (**6**), that also spontaneously precipitated from the aqueous solution. The ^{1}H NMR spectrum of **11** (crystals dissolved in DMSO-d_6) presents eight different bpy resonances, consistent with its asymmetric environment (Figure S8). The 1D NOESY spectrum allowed us to assign the aromatic protons: saturation of the doublet at 9.12 ppm gave an NOE effect with the resonance of the NC*H*$_2$P protons of the PTA (broad singlet centered at 4.32 ppm), thus implying that it belongs to proton H6′, i.e. the one closest to the adjacent PTA. In fact, no NOE effect was observed when the doublet of H6 at 9.16 ppm was saturated. The other bpy resonances were then assigned through an ^{1}H-^{1}H COSY spectrum. The ^{31}P{^{1}H} NMR spectrum presents a singlet at −38.4 ppm, i.e. in the typical region PTA *trans* to bpy. Thus, the NMR data were consistent with the structure. Unfortunately the solution was too diluted for recording an IR spectrum. No attempt was done for maximizing the yield of this side-product.

***trans*-[RuCl$_2$(bpy)(CO)(PTA)] (11).** ^{1}H-NMR (DMSO-d_6) δ 9.16 (d, 1H, H6), 9.12 (d, 1H, H6′), 8.70 (d, 1H, H3'), 8.67 (d, 1H, H3), 8.29 (t, 1H, H4′), 8.19 (t, 1H, H4), 7.84 (t, 1H,

H5′), 7.72 (t, 1H, H5), 4.61, 4.47 (ABq, 6H, NCH_2N), 4.32 (br s, 6H, NCH_2P). ^{13}C NMR from the HSQC spectrum (DMSO-d_6), δ (ppm): 155.7 (C6′), 149.0 (C6), 141.0 (C4′), 139.4 (C4), 128.1 (C5), 127.9 (C5′), 125.0 (C3), 124.8 (C3′), 70.3 (NCH$_2$N), 46.3 (NCH$_2$P). ^{31}P{^{1}H} NMR (DMSO-d_6), δ (ppm): −38.4 (s, 1P, PTA *trans* to bpy).
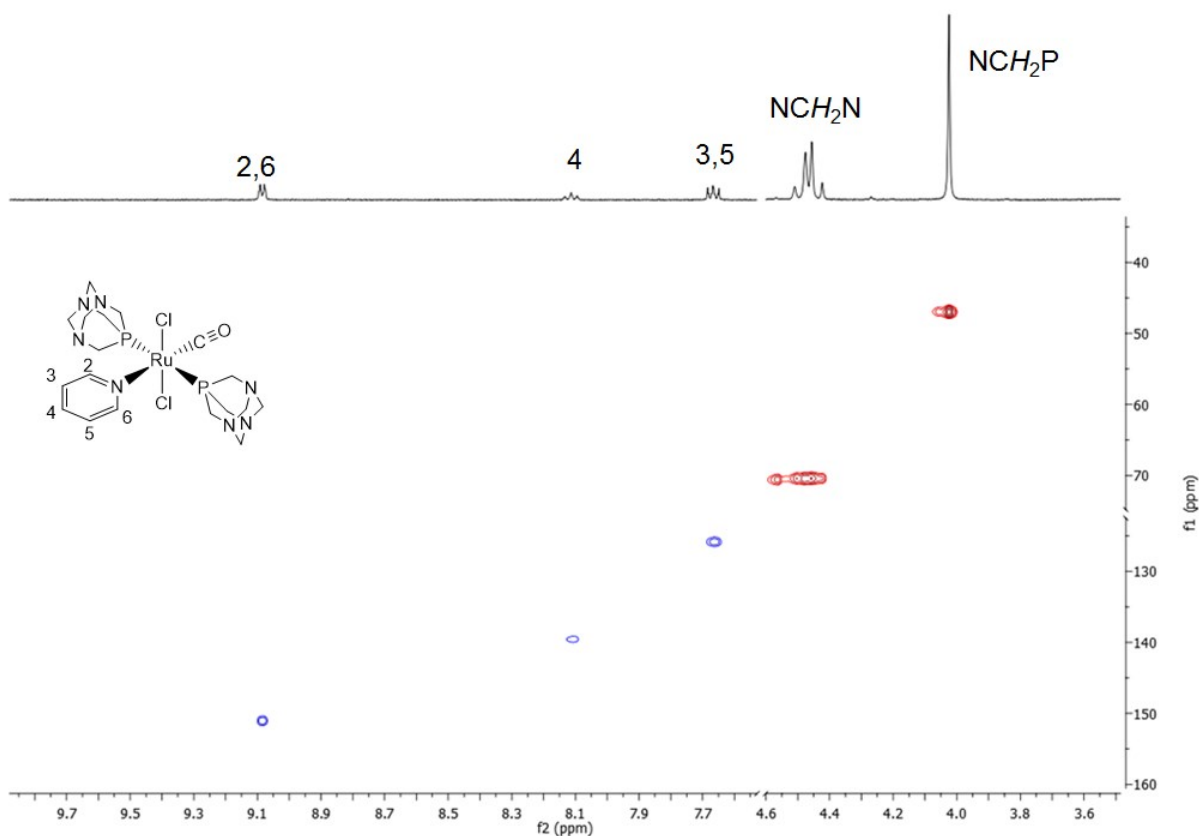
NMR spectra
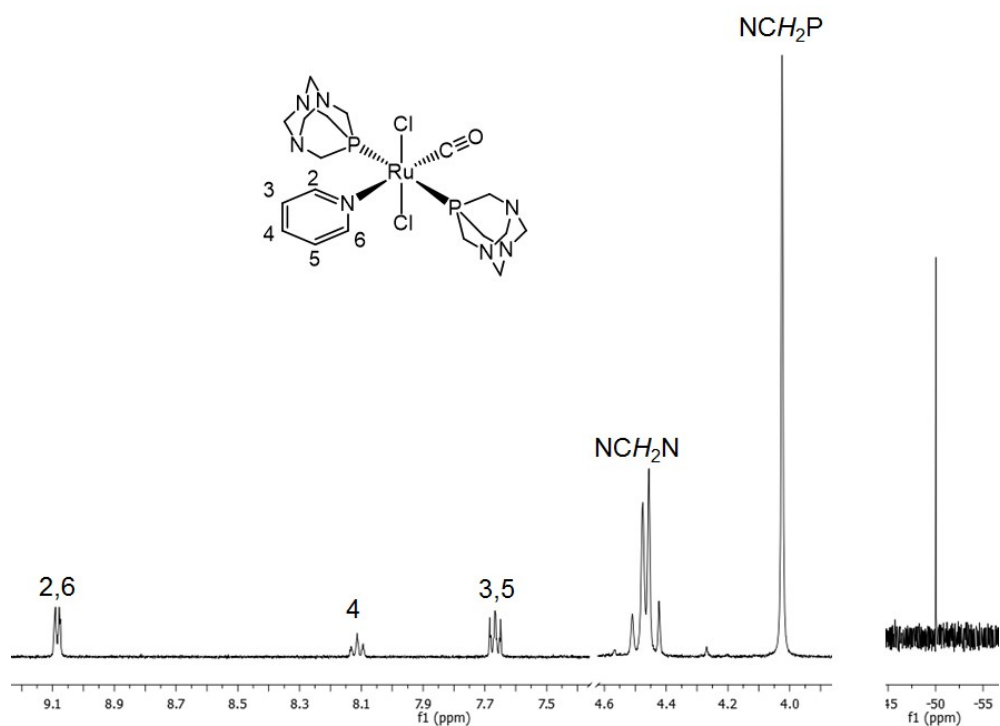
Figure S2. ^{1}H (left) and ^{31}P{^{1}H} (right) NMR spectra of *trans,trans,trans*-[RuCl$_2$(CO)(py)(PTA)$_2$] (**7**) in D$_2$O.
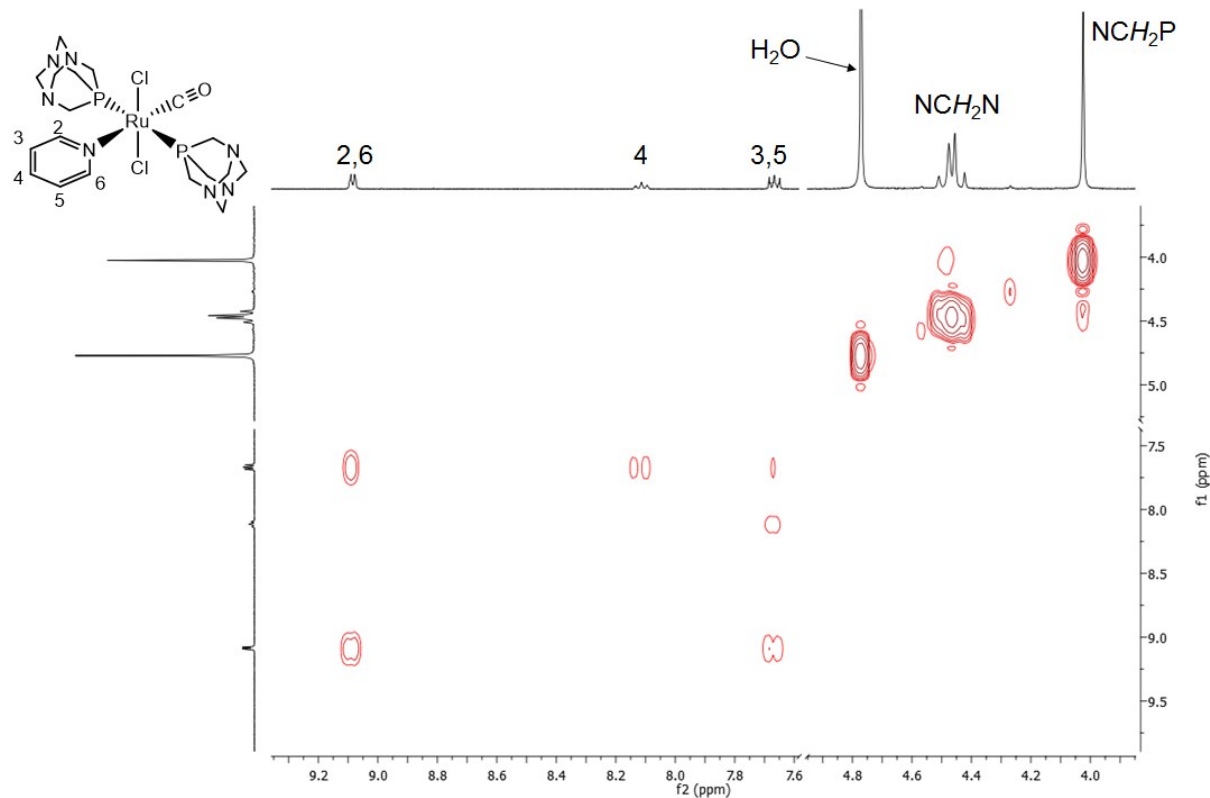
Figure S3. ^{1}H-^{1}H COSY NMR spectrum of *trans,trans,trans*-[RuCl$_2$(CO)(py)(PTA)$_2$] (**7**) in D$_2$O.

Figure S4. ^{1}H-^{13}C HSQC NMR spectrum of *trans,trans,trans*-[RuCl$_2$(CO)(py)(PTA)$_2$] (**7**) in D$_2$O.
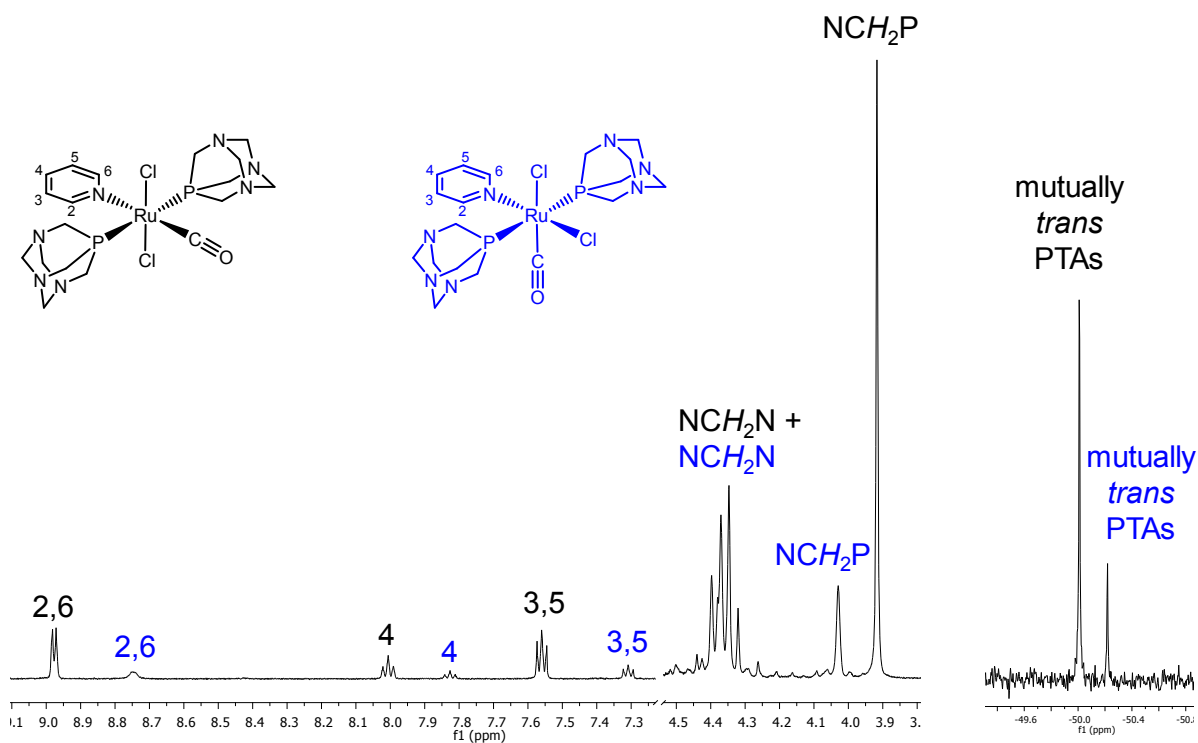
Figure S5. ^{1}H (left) and ^{31}P{^{1}H} (right) NMR spectra in D$_2$O of the mixture of *trans,trans,trans*-[RuCl$_2$(CO)(py)(PTA)$_2$] (**7**, black) and *cis,cis,trans*-[RuCl$_2$(CO)(py)(PTA)$_2$] (**8**, blue) obtained by treatment of **2** with a slight excess of pyridine in chloroform.
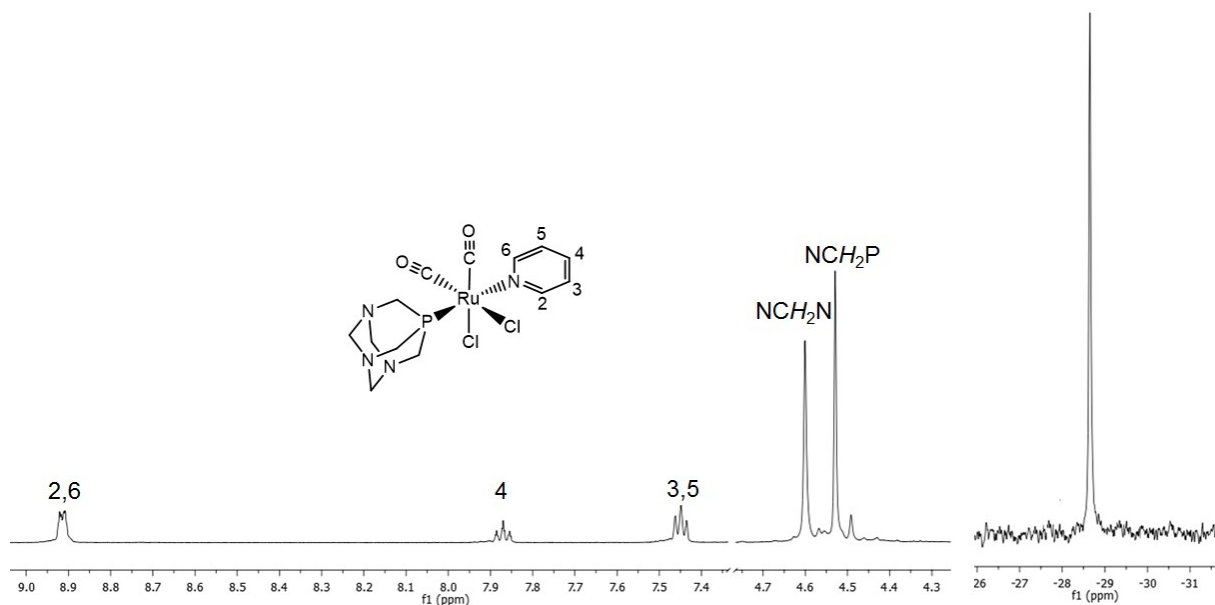
Figure S6. ^{1}H (left) and ^{31}P{^{1}H} (right) NMR spectra of *cis,cis,trans*-[RuCl$_2$(CO)$_2$(py)(PTA)] (**9**) in CDCl$_3$.
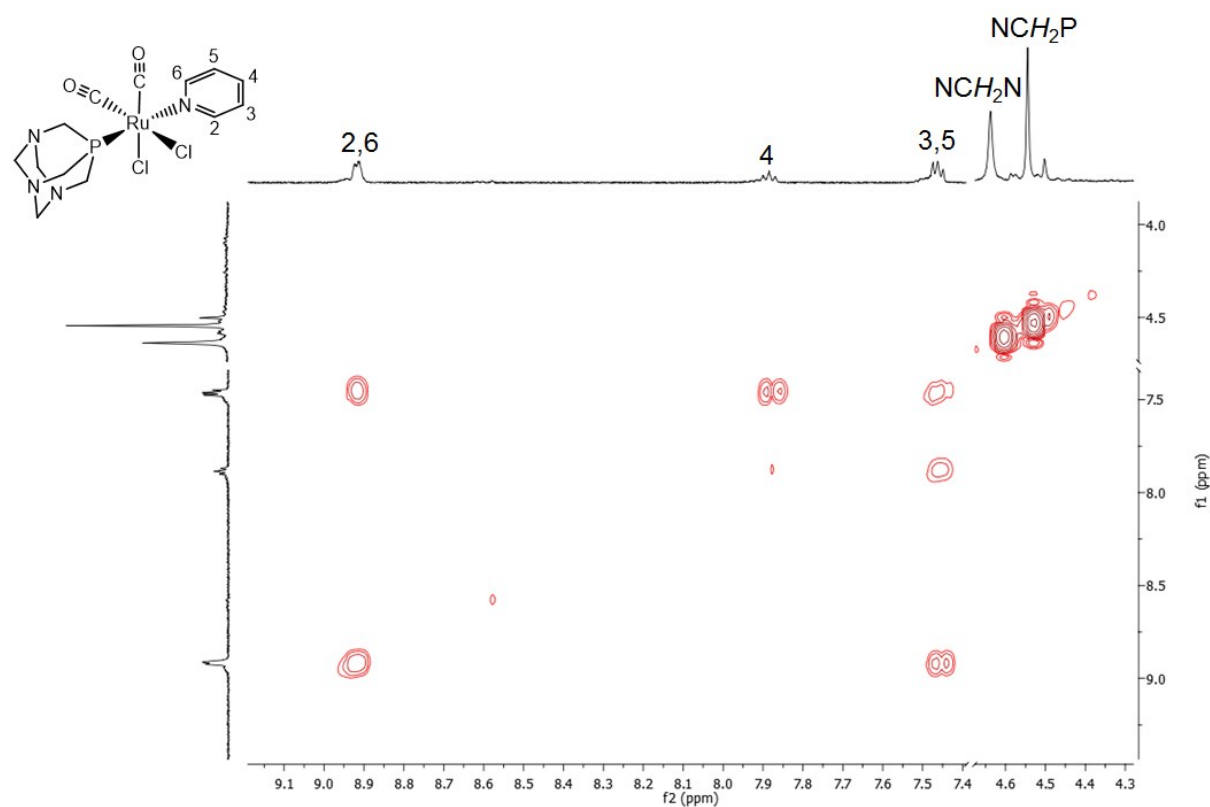
Figure S7. ^{1}H-^{1}H COSY NMR spectrum of *cis,cis,trans*-[RuCl$_2$(CO)$_2$(py)(PTA)] (**9**) in CDCl$_3$.
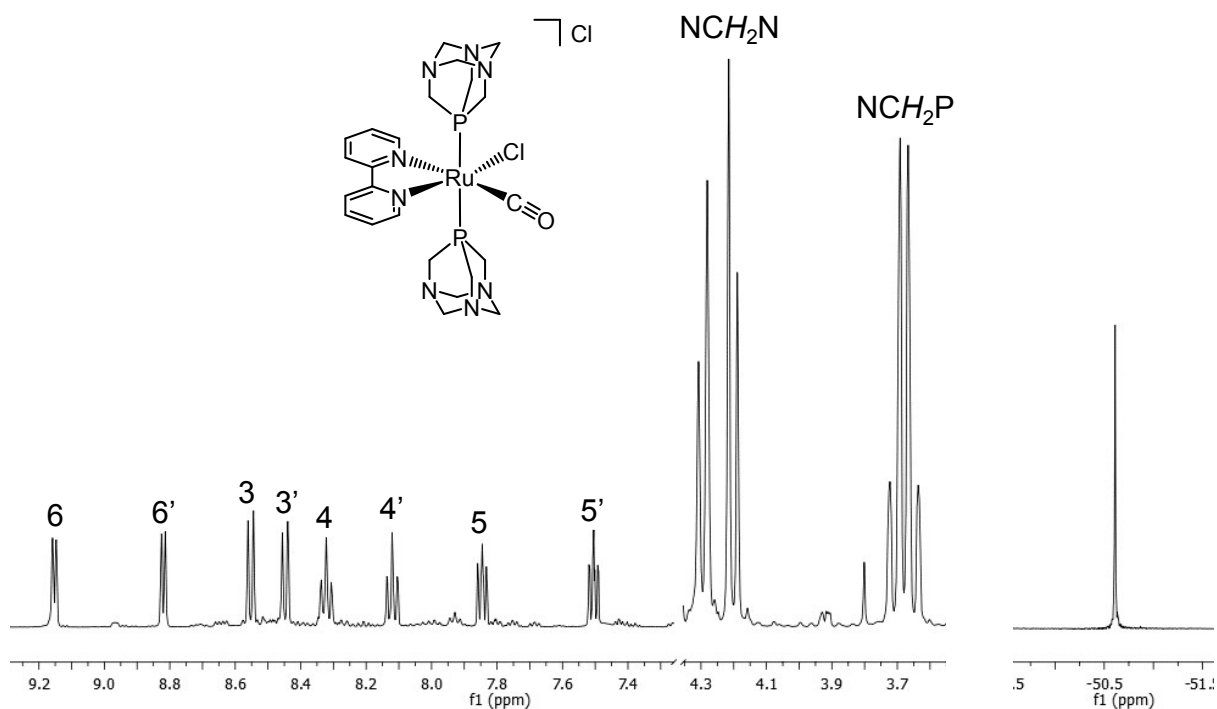
Figure S8. ^1H (left) and $^{31}P\{^1H\}$ (right) NMR spectra of *cis,trans*-[Ru(bpy)Cl(CO)(PTA)$_2$]Cl (**10**) in D$_2$O.
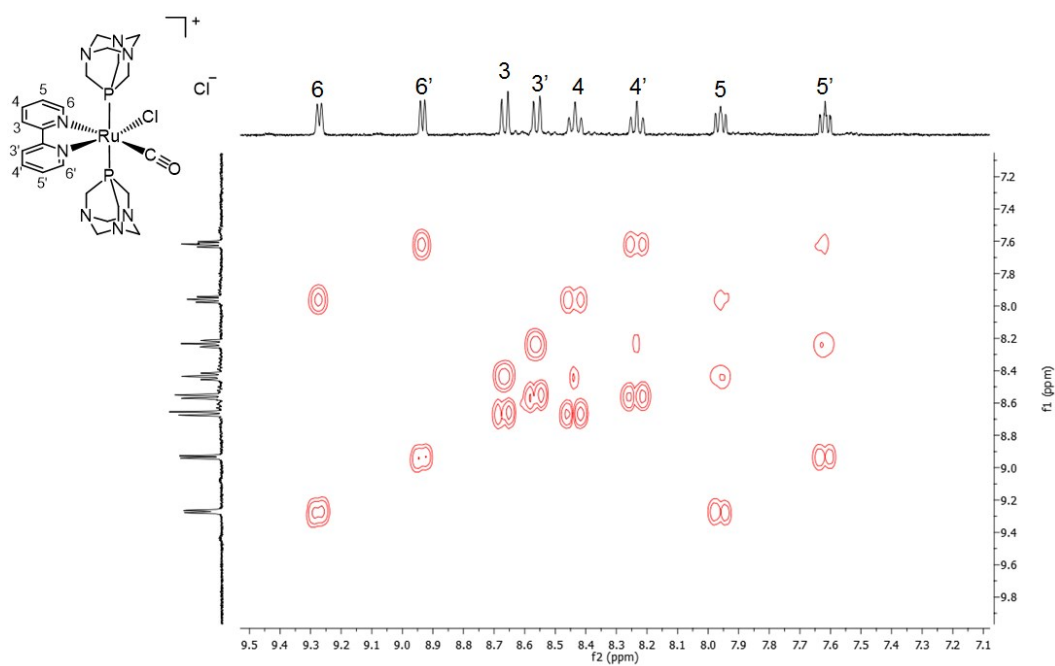
Figure S9. ^1H-^1H COSY NMR spectrum (bpy region) of *cis,trans*-[Ru(bpy)Cl(CO)(PTA)$_2$]Cl (**10**) in D$_2$O.
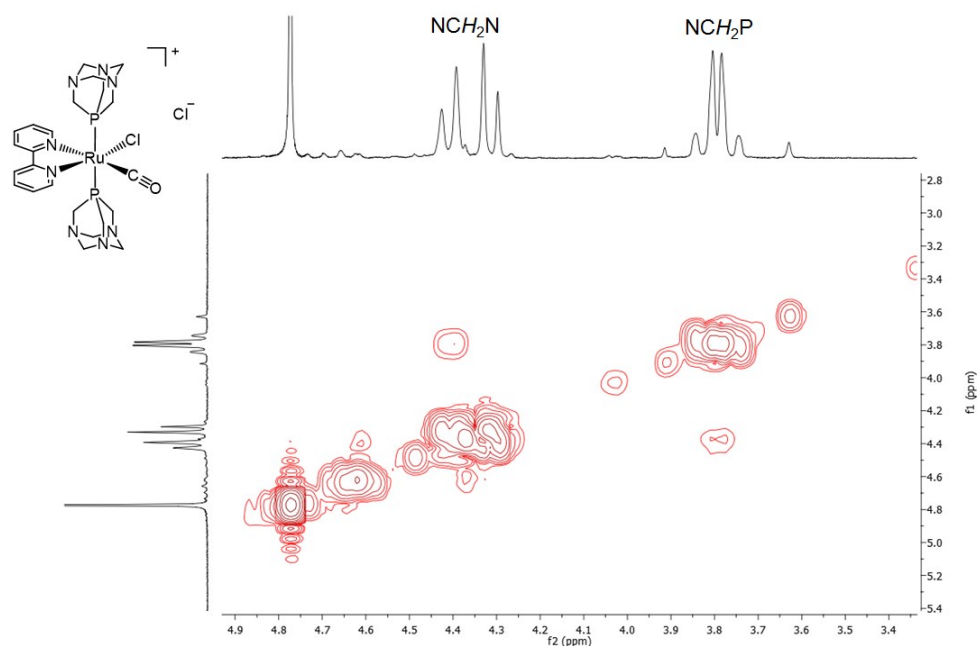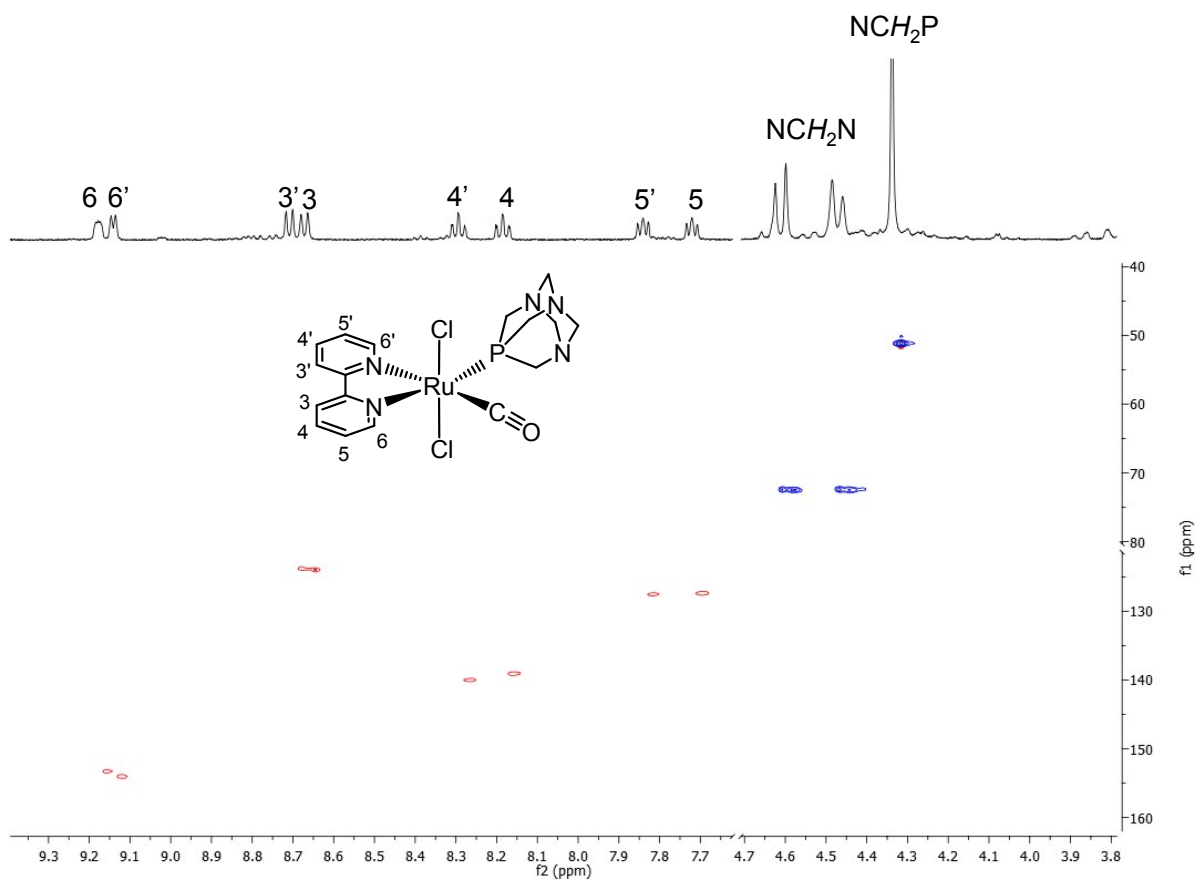
Figure S10. ^{1}H-^{1}H COSY NMR spectrum (PTA region) of *cis,trans*-[Ru(bpy)Cl(CO)(PTA)$_2$]Cl (**10**) in D$_2$O.
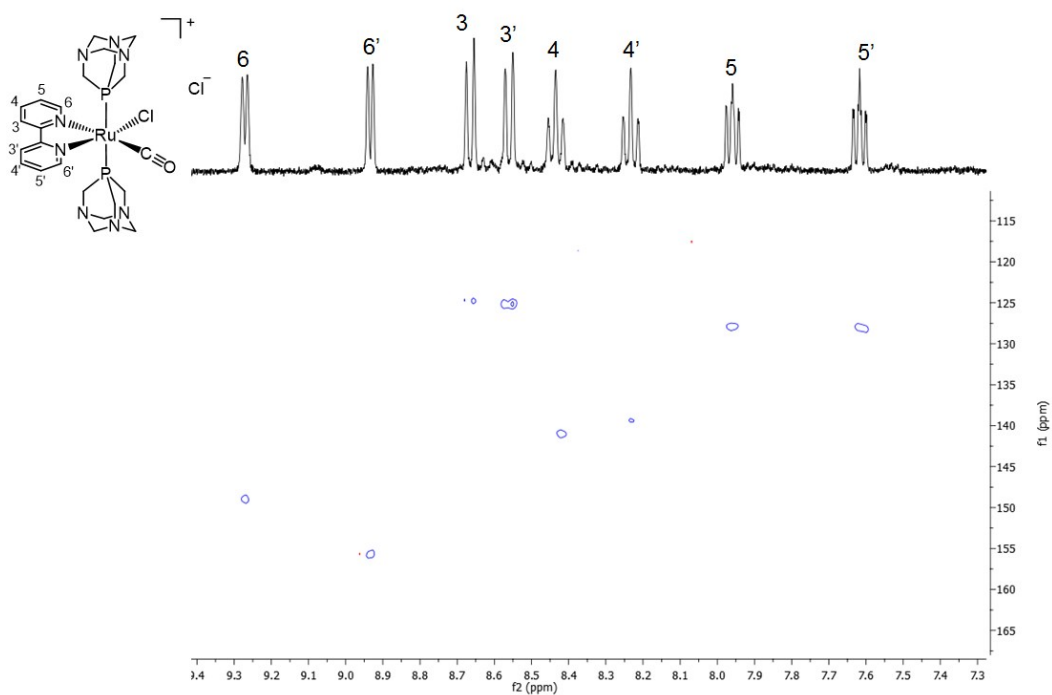
Figure S11. ^{1}H-^{13}C HSQC NMR spectrum (bpy region) of *cis,trans*-[Ru(bpy)Cl(CO)(PTA)$_2$]Cl (**10**) in D$_2$O.
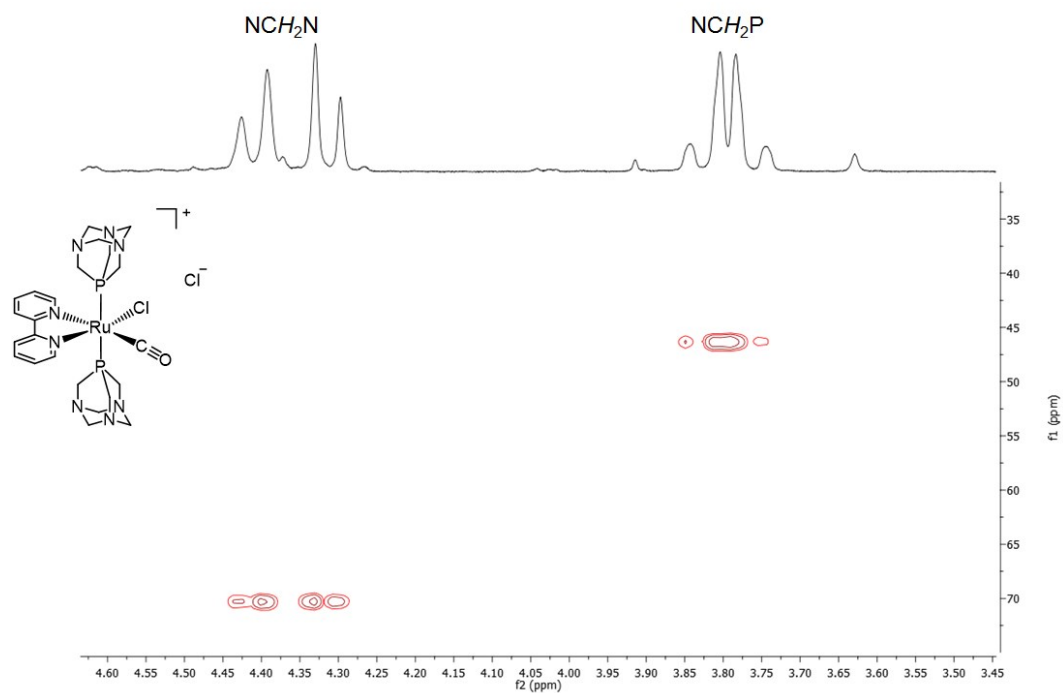
Figure S12. ^{1}H-^{13}C HSQC NMR spectrum (PTA region) of *cis,trans*-[Ru(bpy)Cl(CO)(PTA)$_2$]Cl (**10**) in D$_2$O.
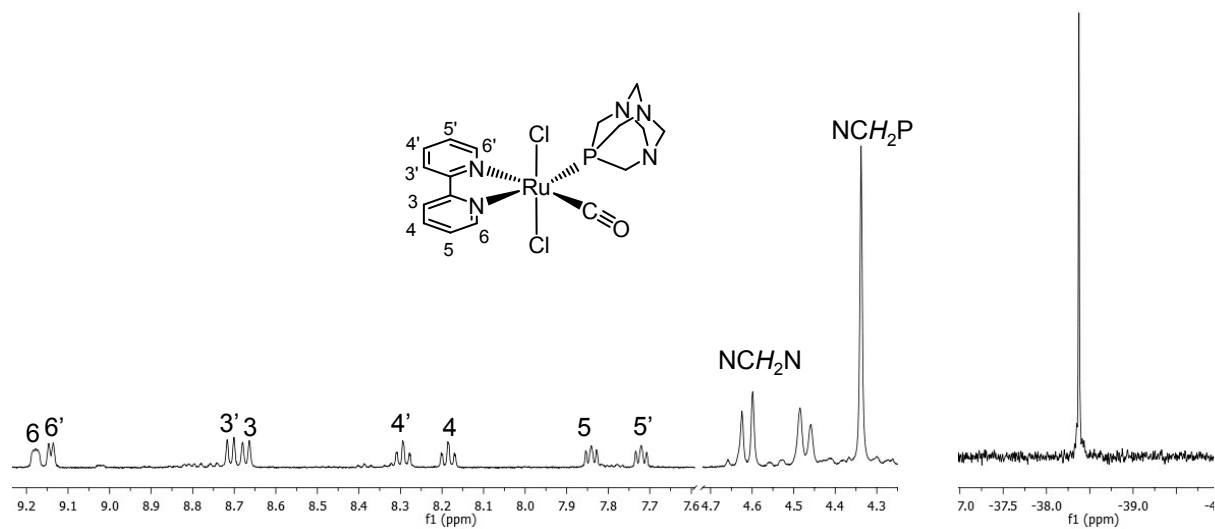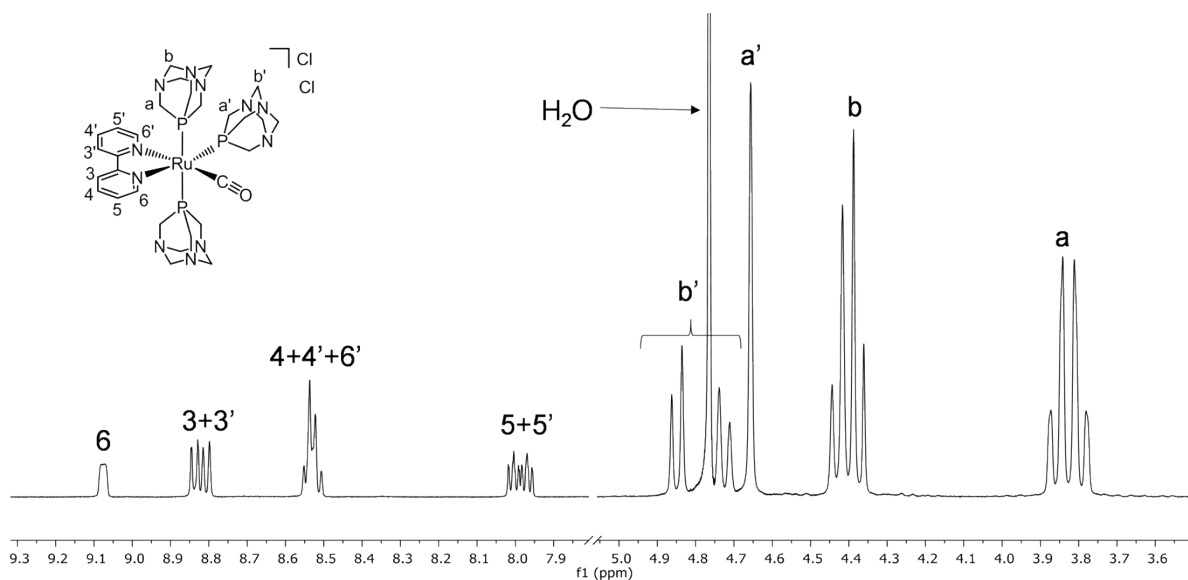

Figure S13. ^{1}H (left) and ^{31}P{^{1}H} (right) NMR spectra of *trans,cis*-[Ru(bpy)Cl$_2$(CO)PTA] (**11**) in DMSO-d_6.
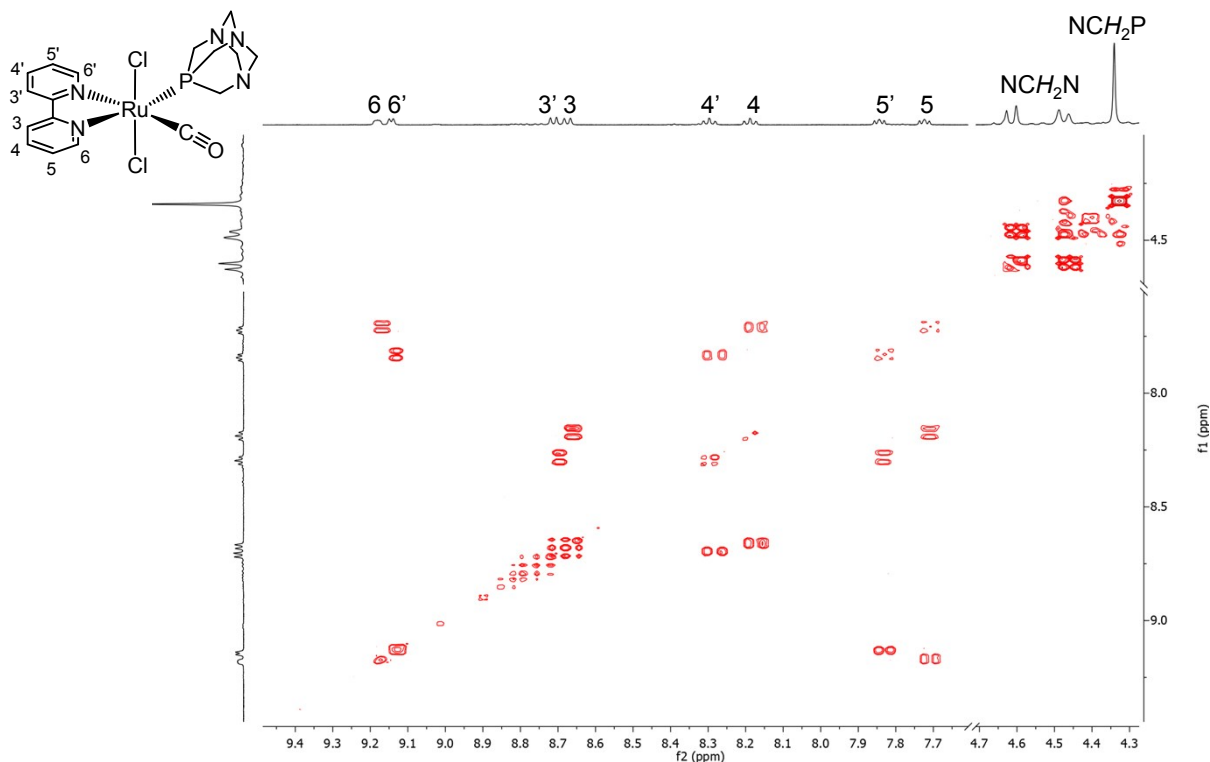
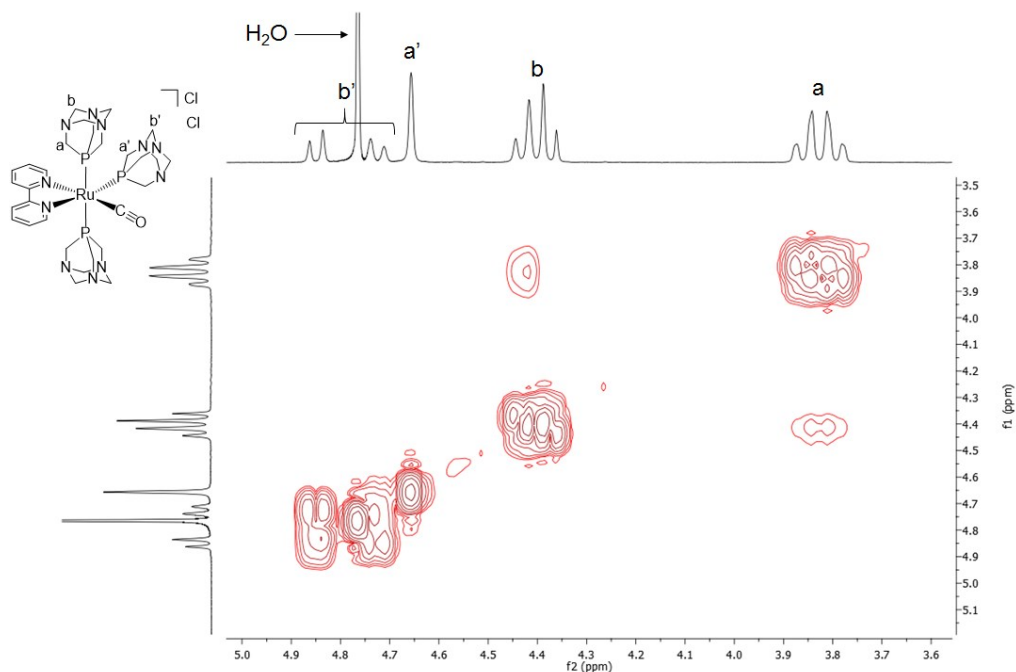**Figure S14.** ^{1}H-^{1}H COSY NMR spectrum of *trans,cis*-[Ru(bpy)Cl$_2$(CO)PTA] (**11**) in DMSO-d_6.

Figure S15. ^{1}H-^{13}C HSQC NMR spectrum of *trans,cis*-[Ru(bpy)Cl$_2$(CO)PTA] (**11**) in DMSO-d_6.
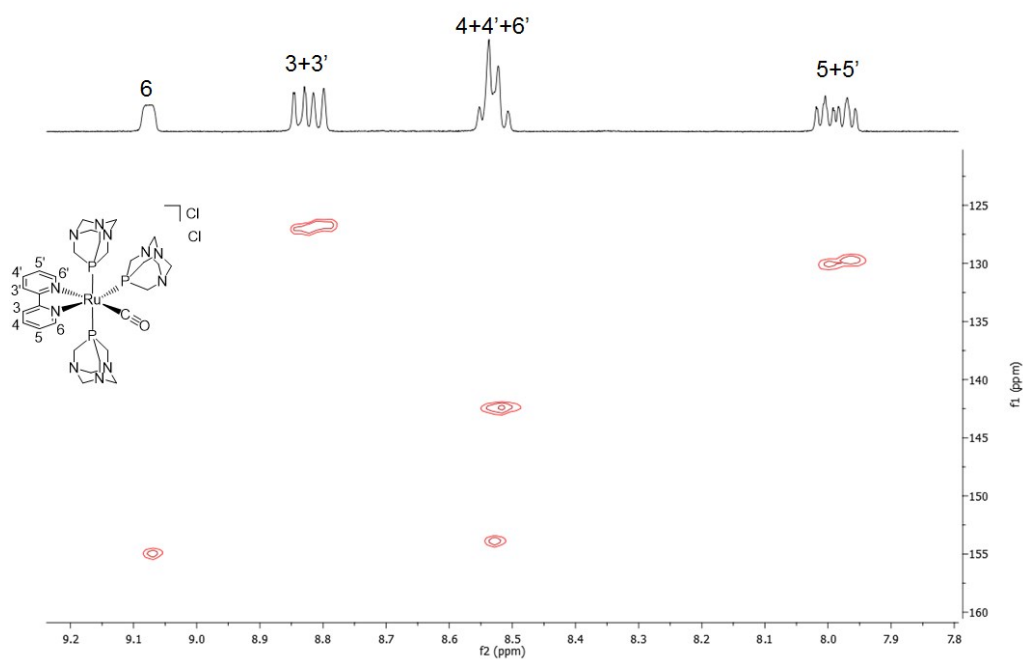
Figure S16. ^{1}H NMR spectrum of *mer*-[Ru(bpy)(CO)(PTA)$_3$]Cl$_2$ (**12**) in D$_2$O.
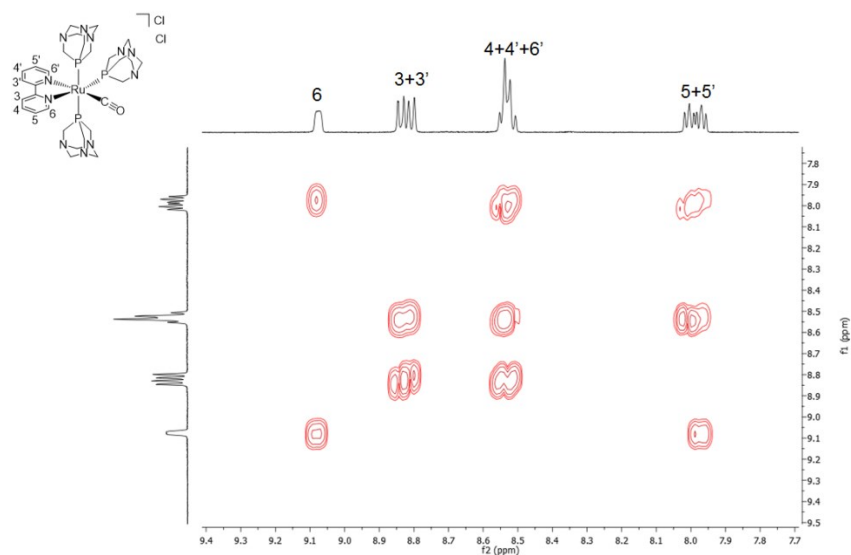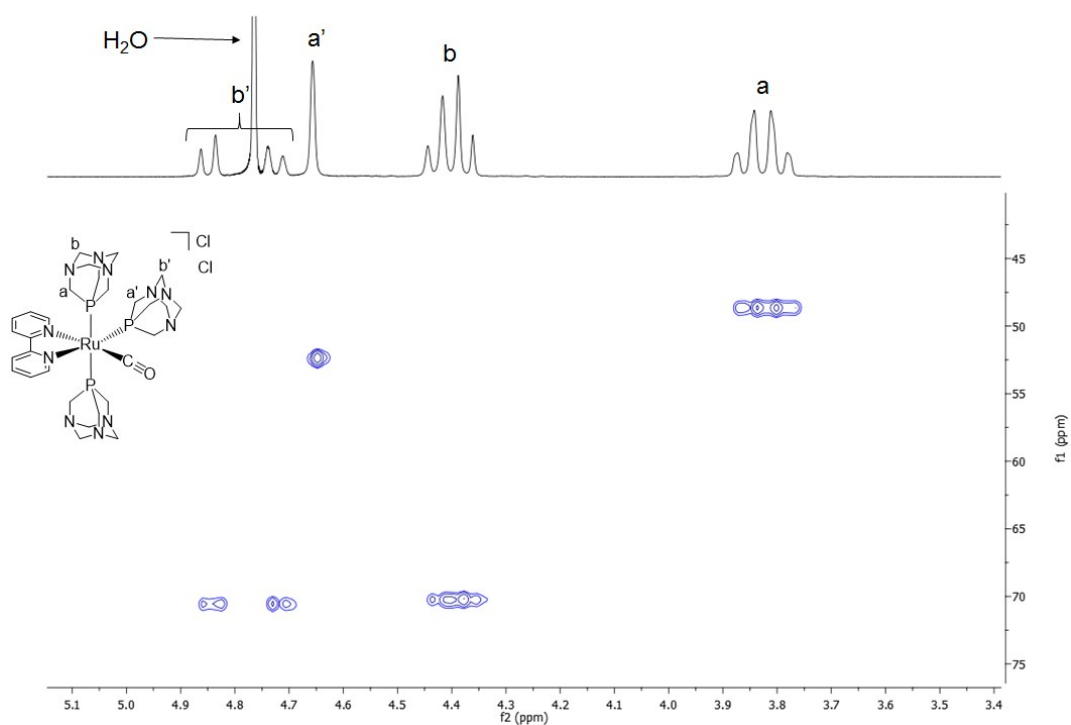

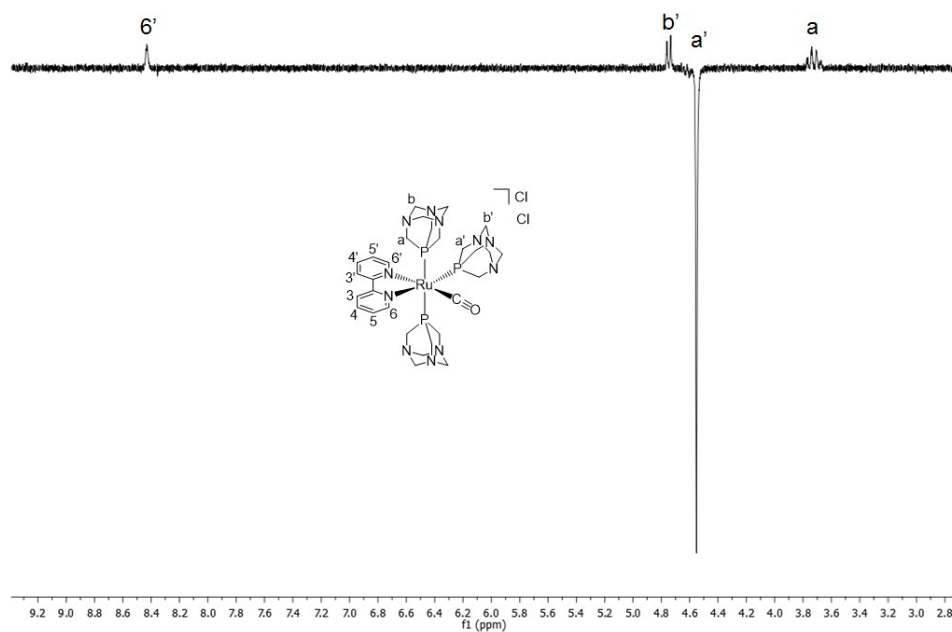**Figure S17.** ^{1}H-^{1}H COSY NMR spectrum (bpy region) of *mer*-[Ru(bpy)(CO)(PTA)$_3$]Cl$_2$ (**12**) in D$_2$O.

Figure S18. ^{1}H-^{1}H COSY NMR spectrum (PTA region) of *mer*-[Ru(bpy)(CO)(PTA)$_3$]Cl$_2$ (**12**) in D$_2$O.

Figure S19. ^{1}H-^{13}C HSQC NMR spectrum (bpy region) of *mer*-[Ru(bpy)(CO)(PTA)$_3$]Cl$_2$ (**12**) in D$_2$O.

Figure S20. ^1H-^{13}C HSQC NMR spectrum (PTA region) of *mer*-[Ru(bpy)(CO)(PTA)$_3$]Cl$_2$ (**12**) in D$_2$O.

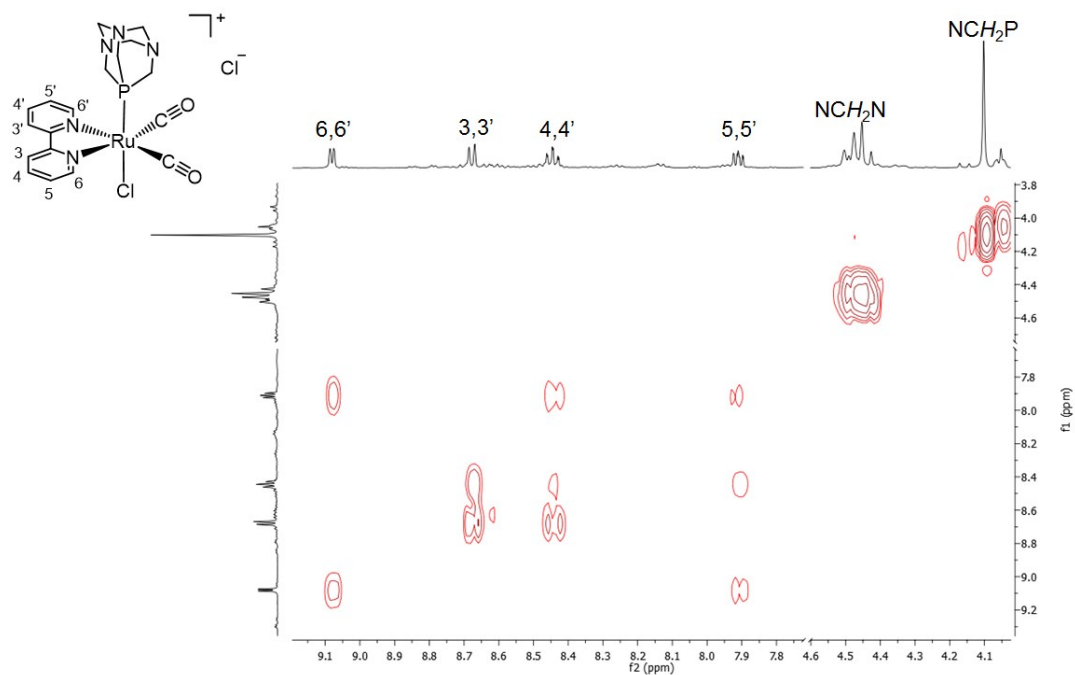**Figure S21.** 1D NOESY NMR spectrum of *mer*-[Ru(bpy)(CO)(PTA)$_3$]Cl$_2$ (**12**) in D$_2$O.
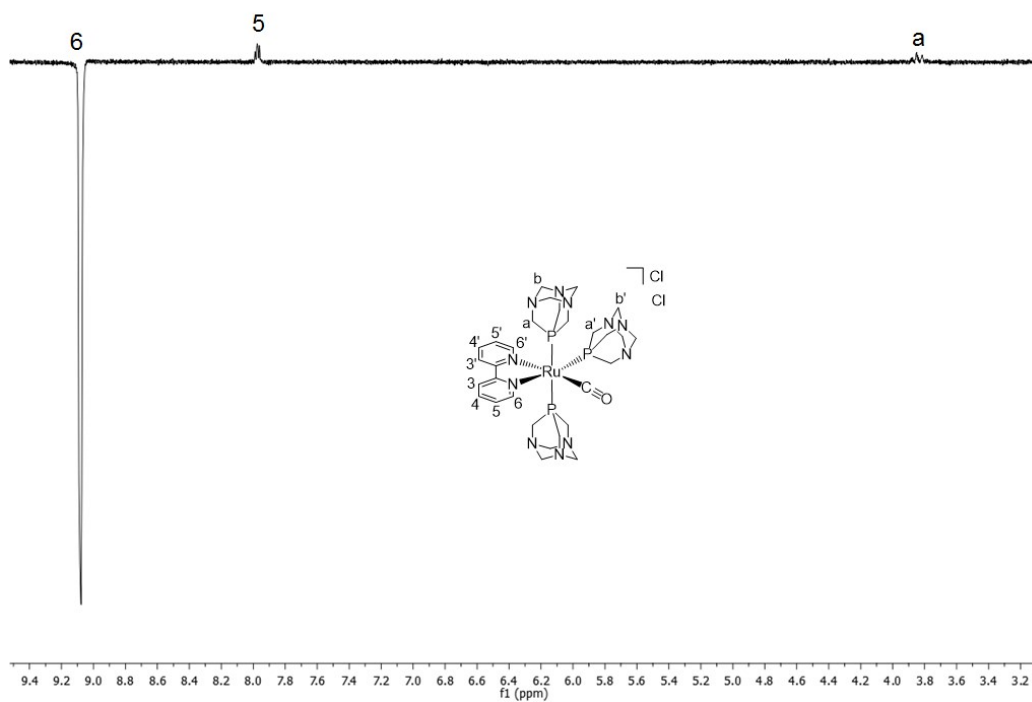
Figure S22. 1D NOESY NMR spectrum of *mer*-[Ru(bpy)(CO)(PTA)₃]Cl₂ (**12**) in D₂O.
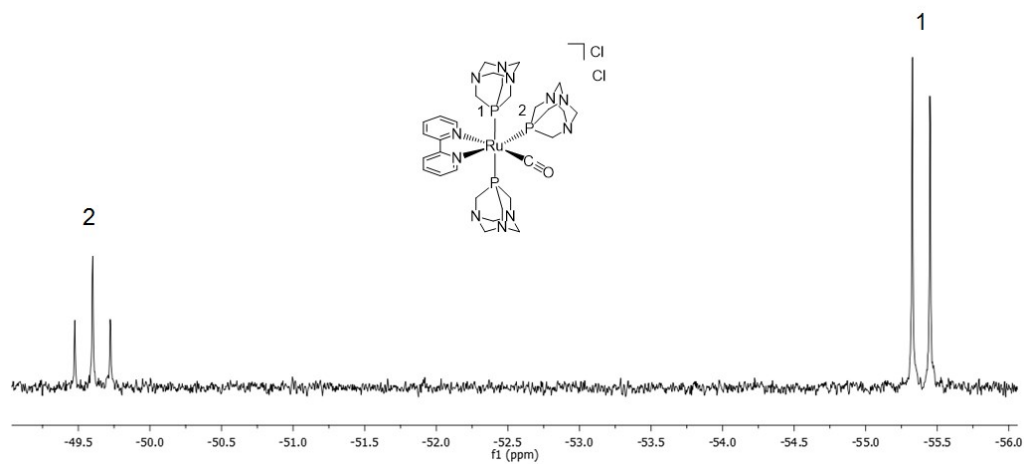
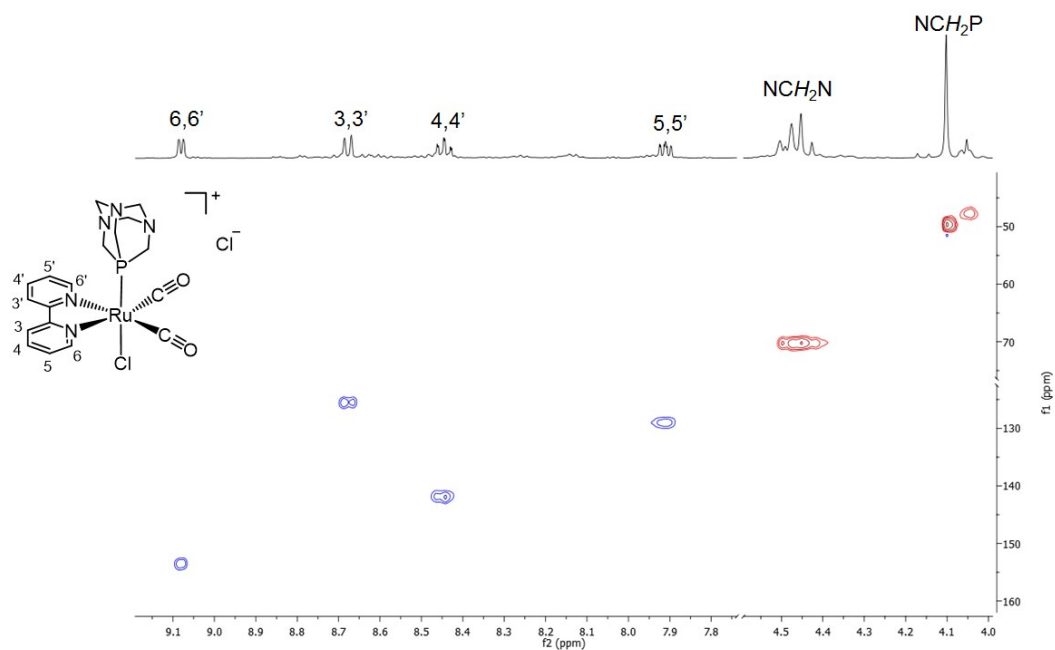**Figure S23.** ³¹P{¹H} NMR spectrum of *mer*-[Ru(bpy)(CO)(PTA)₃]Cl₂ (**12**) in D₂O.
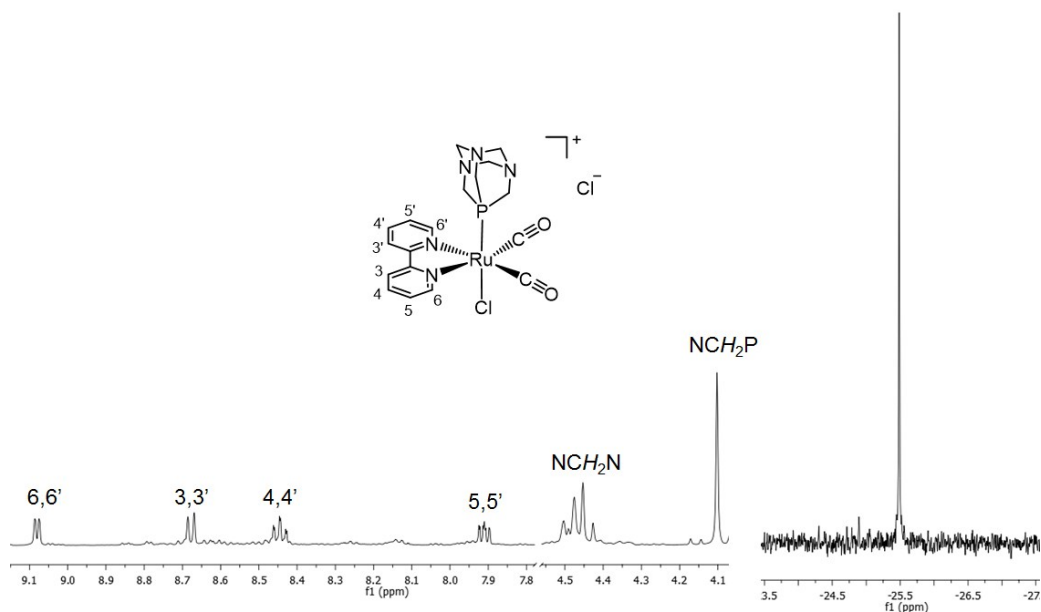
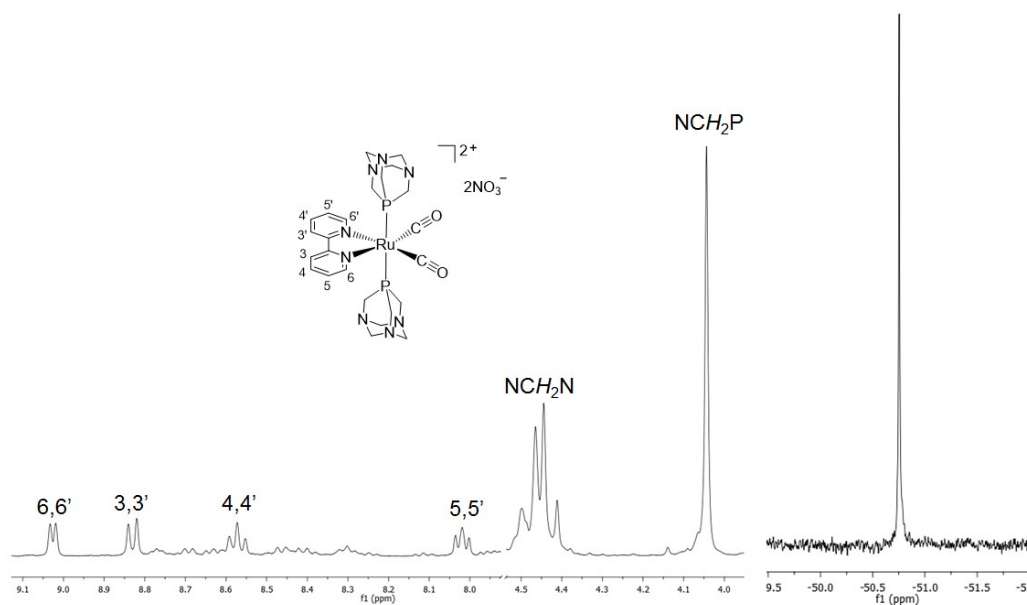**Figure S24.** ^{1}H (left) and ^{31}P{^{1}H} (right) NMR spectra of *cis,trans*-[Ru(bpy)(CO)$_2$Cl(PTA)]Cl (**13**) in D$_2$O.

Figure S25. ^{1}H-^{1}H COSY NMR spectrum of *cis,trans*-[Ru(bpy)(CO)$_2$Cl(PTA)]Cl (**13**) in D$_2$O.

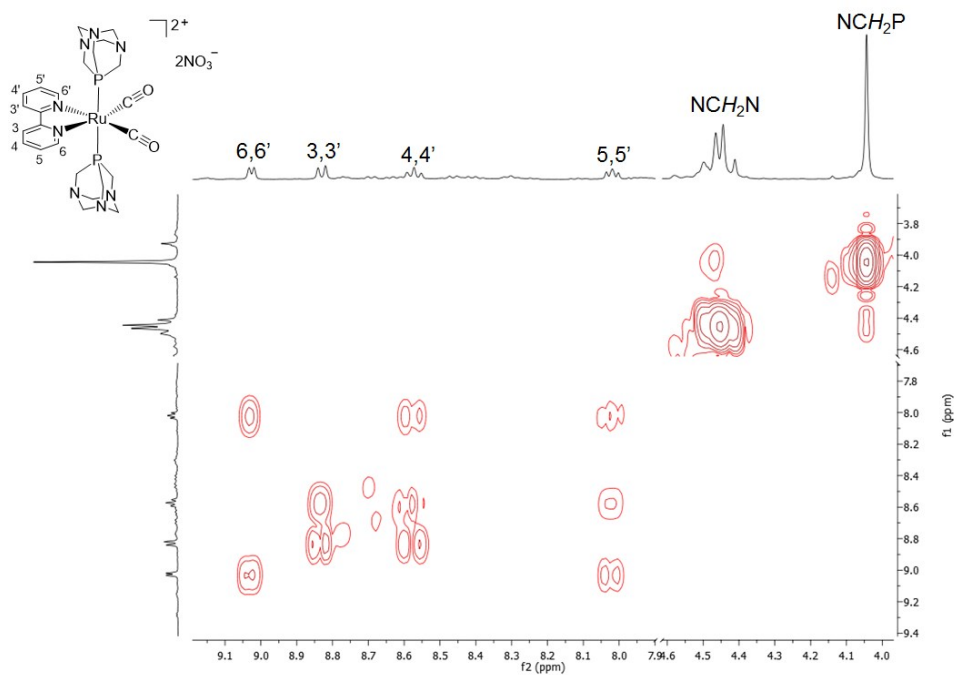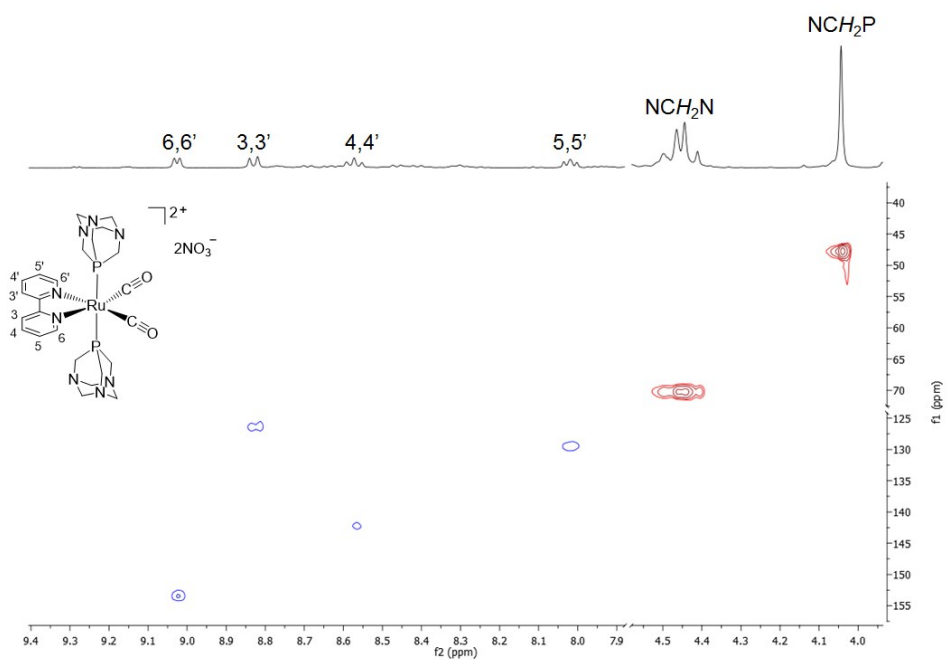**Figure S26.** ^{1}H-^{13}C HSQC NMR spectrum of *cis,trans*-[Ru(bpy)(CO)$_2$Cl(PTA)]Cl (**13**) in D$_2$O.

Figure S27. ^{1}H (left) and ^{31}P{^{1}H} (right) NMR spectra of *cis,trans*-[Ru(bpy)(CO)$_2$(PTA)$_2$](NO$_3$)$_2$ (**14NO$_3$**) in D$_2$O.

Figure S28. ^{1}H-^{1}H HSQC NMR spectrum of *cis,trans*-[Ru(bpy)(CO)$_2$(PTA)$_2$](NO$_3$)$_2$ (**14NO$_3$**) in D$_2$O.

Figure S29. ^{1}H-^{13}C HSQC NMR spectrum of *cis,trans*-[Ru(bpy)(CO)$_2$(PTA)$_2$](NO$_3$)$_2$ (**14NO$_3$**) in D$_2$O.
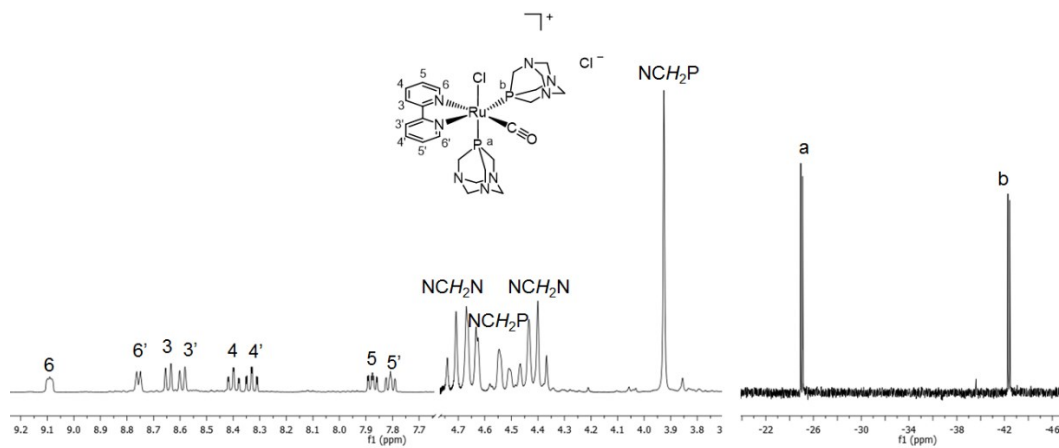
Figure S30. ^{1}H (left) and ^{31}P (right) NMR spectra of *cis,cis*-[Ru(bpy)Cl(CO)(PTA)$_2$]Cl (**15**) in D$_2$O.
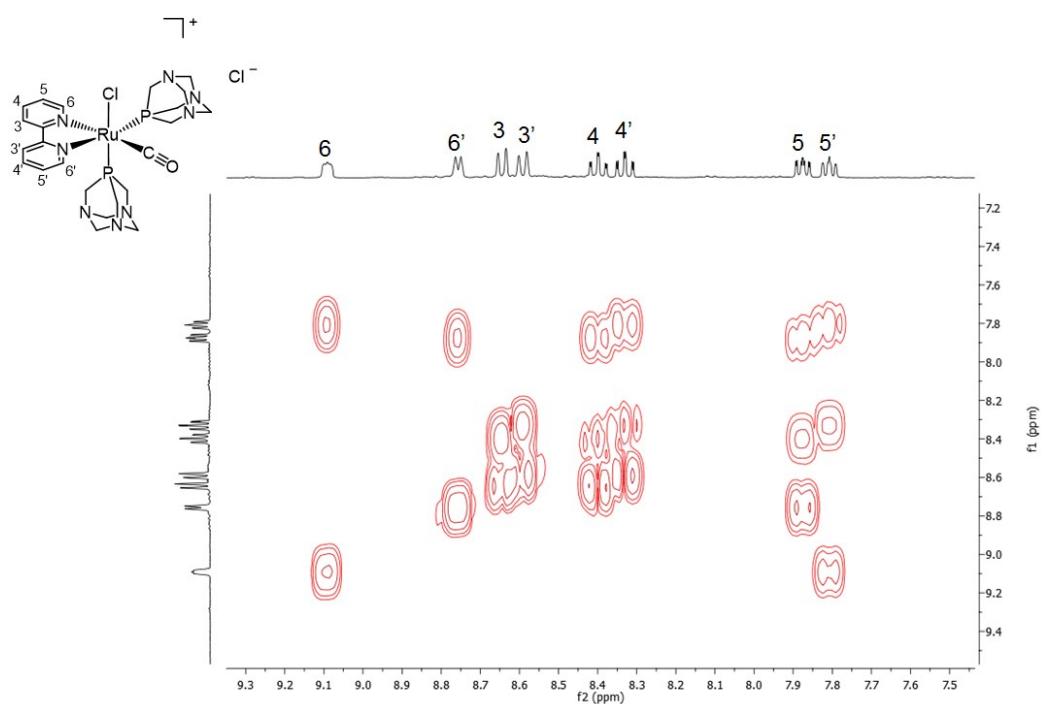
Figure S31. ^{1}H-^{1}H COSY NMR spectrum (bpy region) of *cis,cis*-[Ru(bpy)Cl(CO)(PTA)$_2$]Cl (**15**) in D$_2$O.
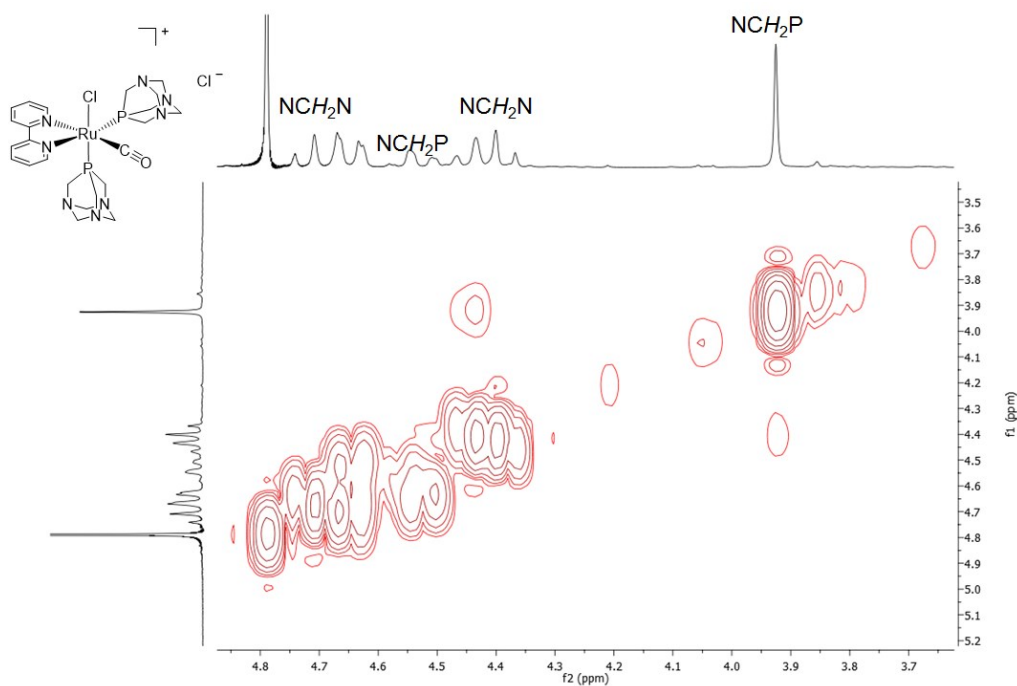
Figure S32. ^{1}H-^{1}H COSY NMR spectrum (PTA region) of *cis,cis*-[Ru(bpy)Cl(CO)(PTA)$_2$]Cl (**15**) in D$_2$O.
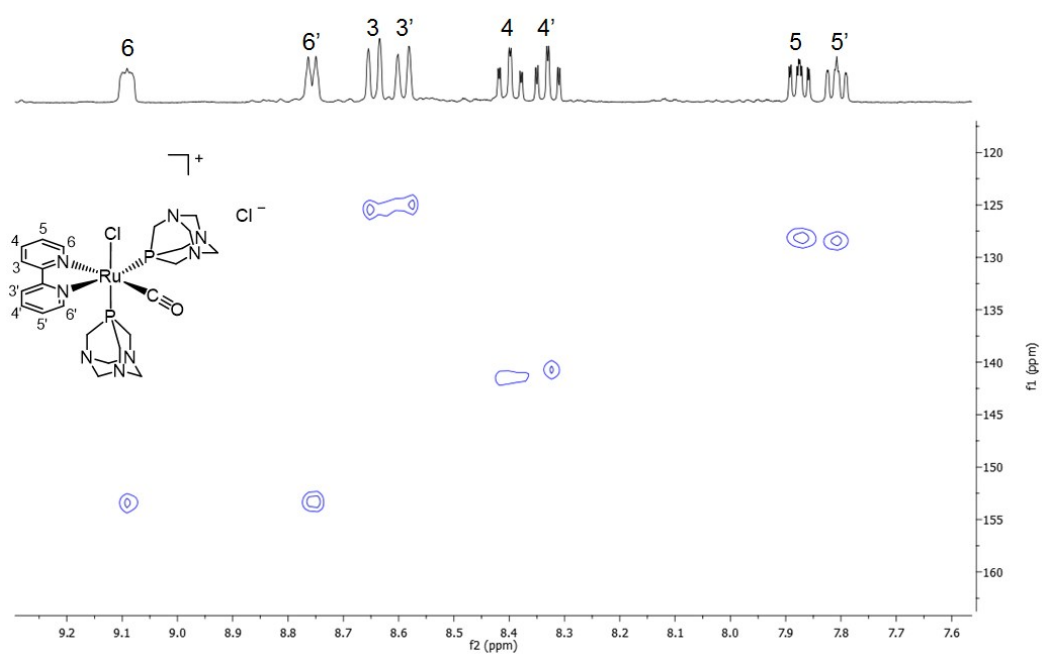
Figure S33. ^{1}H-^{13}C HSQC NMR spectrum (bpy region) of *cis,cis*-[Ru(bpy)Cl(CO)(PTA)$_2$]Cl (**15**) in D$_2$O.
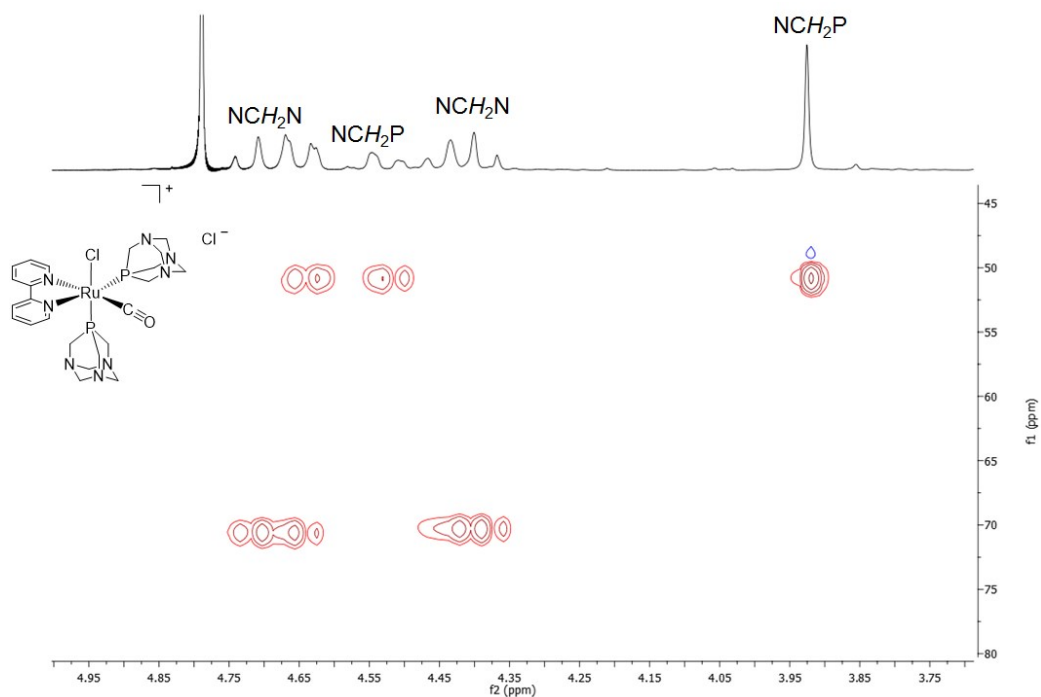
Figure S34. ^{1}H-^{13}C HSQC NMR spectrum (PTA region) of *cis,cis*-[Ru(bpy)Cl(CO)(PTA)$_2$]Cl (**15**) in D$_2$O.
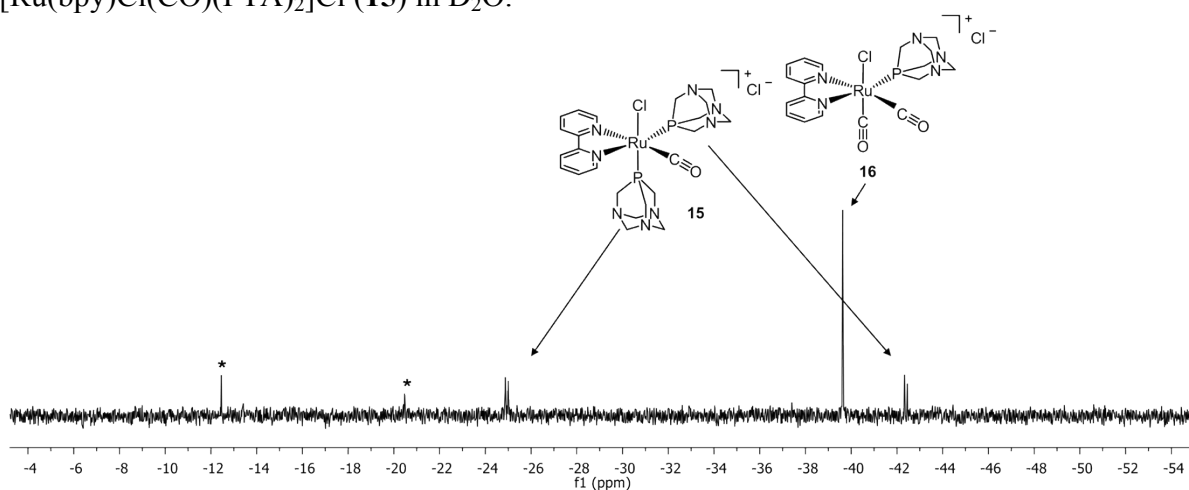
Figure S35. ^{31}P{^{1}H} NMR spectrum in D$_2$O of *cis,cis*-[Ru(bpy)(CO)$_2$Cl(PTA)]Cl (**16**) in 6/1 mixture with *cis,cis*-[Ru(bpy)Cl(CO)(PTA)$_2$]Cl (**15**) and some minor impurities (*).
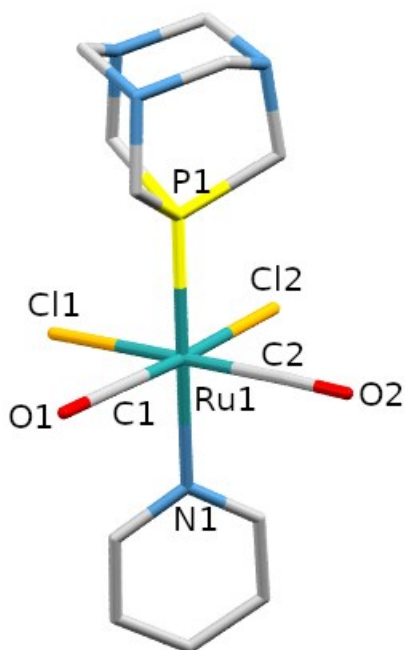
Figure S36. Low-quality X-ray molecular structure (50% probability ellipsoids) of *cis,cis,trans*-[RuCl$_2$(CO)$_2$(py)(PTA)] (**9**).

Table S1 reports the carbonyl stretching bands for complexes **7, 9, 10, 12 – 16**. Those of cationic species fall always at higher wavelengths compared to the corresponding neutral precursor, due to the positive charge(s). With the exception of **9** and **16**, in all the new compounds the COs (either one or two) are always *trans* to py or bpy.

Table S1. CO stretching bands for compounds **7**, **9**, **10**, **12 - 16**. (cm^{-1}).

complex	ν cm^{-1}	CO *trans* to
trans,trans,trans-[RuCl$_2$(CO)(py)(PTA)$_2$] (**7**)	1946[a]	py
cis,cis,trans-[RuCl$_2$(CO)$_2$(py)(PTA)] (**9**)	2058, 1994[b]	Cl
cis,trans-[Ru(bpy)Cl(CO)(PTA)$_2$]Cl (**10**)	1984[c]	bpy
mer-[Ru(bpy)(CO)(PTA)$_3$](Cl)$_2$ (**12**)	2010[a]	bpy
cis,trans-[Ru(bpy)(CO)$_2$Cl(PTA)]Cl (**13**)	2085, 2034[d]	bpy
cis,trans-[Ru(bpy)(CO)$_2$(PTA)$_2$](NO$_3$)$_2$ (**14NO$_3$**)	2086, 2038[d]	bpy
cis,cis-[Ru(bpy)Cl(CO)(PTA)$_2$]Cl (**15**)	1992[c]	bpy
cis,cis-[Ru(bpy)(CO)$_2$Cl(PTA)]Cl (**16**)	2006, 1979[c]	bpy/Cl

[a] Solid state (nujol mull); [b] Chloroform solution, [c] EtOH solution, [d] MeOH solution.

Table S2. Crystallographic data and refinement details for compounds *trans,trans,trans*-[RuCl$_2$(CO)(py)(PTA)$_2$] (**7**) and *trans*-[Ru(bpy)Cl$_2$(CO)PTA]·H$_2$O (**11**·H$_2$O).

	7	**11**·H$_2$O
Empirical Formula	C$_{18}$H$_{29}$N$_7$Cl$_2$OP$_2$Ru	C$_{17}$H$_{20}$N$_5$Cl$_2$OPRu·H$_2$O
Formula weight (Da)	593.39	531.33
Temperature (K)	100(2)	100(2)
Wavelength (Å)	0.700	0.700
Crystal system	orthorhombic	monoclinic
Space Group	*P* 21 21 21	*P* 21/c
a (Å)	7.361(1)	6.80(1)
b (Å)	16.841(1)	21.768(5)
c (Å)	19.166(2)	13.521(3)
α (°)	90	90
β (°)	90	94.77(2)
γ (°)	90	90
V (Å^3)	2375.9(5)	1994(3)
Z	4	4
ρ (g·cm^{-3})	1.659	1.770
F(000)	1208	1072
μ (mm^{-1})	0.990	1.097
θ min, max (°)	1.585, 33.088	1.751, 33.091
Resolution (Å)	0.64	0.64
Total refl. collctd	48334	41070
Independent refl.	8401	6828
Obs. Refl. [Fo>4σ(Fo)]	8337	6754
I/σ(I) (all data)	107.33	33.20
I/σ(I) (max res)	34.87	19.03
Completeness (all data)	0.981	0.998
R$_{merge}$ (all data)	1.4%	4.7%
R$_{merge}$ (max res)	1.6%	3.3%
Multiplicity (all data)	10.2	6.0
Multiplicity (max res)	2.6	2.5
Data/restraint/parameters	8401/0/312	6828/29/321
GooF	1.034	1.007
R[I>2.0σ(I)],[a] wR2 [I>2.0σ(I)][a]	0.0376, 0.1114	0.0278, 0.0805
R (all data),[a] wR2 (all data)[a]	0.0378, 0.1115	0.0279, 0.0807

[a]$R_1 = \Sigma \,|Fo|-|Fc|| \,/\, \Sigma|Fo|$, $wR_2 = [\Sigma\, w\, (Fo^2 - Fc^2\,)^2 \,/\, \Sigma w\, (Fo^2\,)^2]^{1/2}$

Table S2 contd. Crystallographic data and refinement details for compounds *mer*-[Ru(bpy)(CO)(PTA)$_3$]Cl$_2$·7H$_2$O (**12**·7H$_2$O).

	12·7H$_2$O
Empirical Formula	C$_{29}$H$_{44}$N$_{11}$Cl$_2$OP$_3$Ru·7H$_2$O
Formula weight (Da)	953.74
Temperature (K)	100(2)
Wavelength (Å)	0.700
Crystal system	monoclinic
Space Group	*P* 21/c
a (Å)	12.784(5)
b (Å)	13.5660(12)
c (Å)	23.229(3)
α (°)	90
β (°)	103.121(5)
γ (°)	90
V (Å^3)	3923.4(18)
Z	4
ρ (g·cm^{-3})	1.615
F(000)	1984
μ (mm^{-1})	0.683
θ min, max (°)	1.611, 29.085
Resolution (Å)	0.72
Total refl. collctd	132580
Independent refl.	10889
Obs. Refl. [Fo>4σ(Fo)]	10849
I/σ(I) (all data)	55.60
I/σ(I) (max res)	49.59
Completeness (all data)	0.986
R$_{merge}$ (all data)	3.9%
R$_{merge}$ (max res)	3.8%
Multiplicity (all data)	11.9
Multiplicity (max res)	10.3
Data/restraint/parameters	10889/25/530
GooF	0.967
R[I>2.0σ(I)],[a] wR2 [I>2.0σ(I)][a]	0.0242, 0.0701
R (all data),[a] wR2 (all data)[a]	0.0243, 0.0702

[a]$R_1 = \Sigma \, |Fo|-|Fc|| \, / \, \Sigma|Fo|$, $wR_2 = [\Sigma \, w \, (Fo^2 - Fc^2 \,)^2 \, / \, \Sigma w \, (Fo^2 \,)^2]^{\frac{1}{2}}$

Table S3. Selected coordination distances (Å) and angles (°) for *trans,trans,trans*-[RuCl$_2$(CO)(py)(PTA)$_2$] (**7**).

Bond distances (Å)			
Ru1–C36[a]	1.861(7)	Ru1–P2	2.344(1)
Ru1–Cl1	2.409(1)	Ru1–Cl2	2.419(1)
Ru1–P1	2.349(1)	Ru1–N3[a]	2.207(6)
Ru1–C46[b]	1.90(3)	Ru1–N4[b]	2.18(3)
Bond angles (°)			
Cl1–Ru1–Cl2	179.47(5)	P2–Ru1–Cl1	90.62(4)
P1–Ru1–P2	179.35(5)	N3–Ru1–P2[a]	88.4(2)
N3–Ru1–Cl1[a]	91.2(2)	C36–Ru1–Cl1[a]	91.7(2)
N3–Ru1–Cl2[a]	88.5(2)	C36–Ru1–Cl2[a]	88.5(2)
N3–Ru1–P1[a]	91.1(2)	C36–Ru1–P1[a]	91.3(2)
P1–Ru1–Cl1	88.93(4)	C36–Ru1–P2[a]	89.2(2)
P1–Ru1–Cl2	90.62(4)	C36–Ru1–N3[a]	176.3(3)
P2–Ru1–Cl2	89.83(4)	N4–Ru1–Cl1[b]	86.5(9)
N4–Ru1–Cl2[b]	93.7(9)	C46–Ru1–Cl1[b]	84(1)
N4–Ru1–P1[b]	88.7(8)	C46–Ru1–Cl2[b]	96(1)
N4–Ru1–P2[b]	91.8(8)	C46–Ru1–P1[b]	86.0(8)
C46–Ru1–P2[b]	93.4(8)	C46–Ru1–N4[b]	169(2)

[a]Major population (74.7%); [b]Minor population (25.3%)

Table S4. Selected coordination distances (Å) and angles (°) for *trans*-[Ru(bpy)Cl$_2$(CO)PTA]·H$_2$O (**11**·H$_2$O).

Bond distances (Å)			
Ru1–C1	1.842(2)	Ru1–P2	2.305(1)
Ru1–Cl1	2.417(2)	Ru1–N31	2.134(2)
Ru1–Cl2	2.402(1)	Ru1–N32	2.154(1)
Bond angles (°)			
C1–Ru1–Cl1	87.71(7)	N31–Ru1–Cl1	91.18(6)
C1–Ru1–Cl2	96.62(7)	N31–Ru1–Cl2	88.24(6)
C1–Ru1–P2	88.09(6)	N31–Ru1–P2	174.09(3)
C1–Ru1–N31	95.82(7)	N31–Ru1–N32	76.77(7)
C1–Ru1–N32	169.83(5)	N32–Ru1–Cl1	85.52(6)
P2–Ru1–Cl1	93.41(6)	N32–Ru1–P2	99.88(6)
P2–Ru1–Cl2	86.90(5)	N32–Ru1–Cl2	90.17(6)
Cl1–Ru1–Cl2	175.66(1)		

Table S5. Selected coordination distances (Å) and angles (°) for *mer*-[Ru(bpy)(CO)(PTA)$_3$]Cl$_2 \cdot$7H$_2$O (**12**$\cdot$7H$_2$O).

Bond distances (Å)			
Ru1–C1	1.8746(14)	Ru1–P4	2.3631(4)
Ru1–P2	2.3650(4)	Ru1–N51	2.119(1)
Ru1–P3	2.3391(4)	Ru1–N52	2.139(1)
Bond angles (°)			
C1–Ru1–N51	97.31(5)	N51–Ru1–P2	85.90(3)
C1–Ru1–N52	174.37(4)	N51–Ru1–P3	175.25(3)
C1–Ru1–P2	92.57(4)	N51–Ru1–P4	86.58(3)
C1–Ru1–P3	87.19(4)	N51–Ru1–N52	77.06(4)
C1–Ru1–P4	88.04(4)	N52–Ru1–P2	87.10(3)
P2–Ru1–P3	95.44(1)	N52–Ru1–P3	98.44(3)
P2–Ru1–P4	172.47(1)	N52–Ru1–P4	91.56(3)
P3–Ru1–P4	92.08(1)		